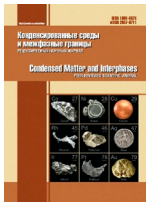

ISSN 1606-867X (Print)
ISSN 2687-0711 (Online)
Condensed Matter and Interphases
Kondensirovannye Sredy i Mezhfaznye Granitsy
https://journals.vsu.ru/kcmf/

Original articles

Research article
http://doi.org/10.17308/kcmf.2025.27/12489

Topography and microrelief electroless Ni-P coatings at different loading densities

I. V. Petukhov✉, **N. A. Medvedeva**

Perm State University,
15 ul. Bukireva, Perm 614990, Russian Federation

Abstract

The aim of this study was to investigate the growth processes of Ni-P coatings at different loading densities of the electroless nickel plating bath. The Ni-P coatings can be used to improve the thermal and corrosion resistance of optical fiber used to manufacture sensors of various physical quantities.

When depositing coatings on optical fiber, the loading density is an important parameter. The study investigated the influence of loading density on the topography, microrelief, roughness, and growth mechanism of Ni-P coatings using non-contact high-resolution optical profilometry. An increase in loading density from 0.5 to 3.0 dm^2/l did not lead to a significant change in the roughness parameters of the coatings. During the growth of coatings, "spheroids" strongly elongated in the plane of the substrate were formed on the surface. An analysis of growth processes was carried out within the framework of the layered growth mechanism. The growth rates of spheroids in normal and lateral directions were assessed. An increase in the loading density led to a decrease in the growth of spheroids in the normal direction, while the growth rate in the lateral direction was maximal at a loading density of 2 dm^2/l. Statistical analysis of the sizes of the "spheroids" showed that their distribution deviated from the normal law, which may be due to the fact that not only individual spheroids, but also their aggregates were considered in calculations. Another reason for the deviation may be a decrease in the proportion of the active surface on which the coating is deposited as the loading density increases.

Since increasing the loading density from 0.5 to 3.0 dm^2/l did not lead to a significant change in the roughness parameters even with coating thickness of ~ 8 μm or higher; deposition of coatings with the thickness up to 3.5 μm thick on optical fibers can be carried out at the specified loading densities with acceptable surface roughness.

Keywords: Optical fiber, Ni-P coatings, Electroless deposition, Non-contact profilometry, Topography, Microrelief, Roughness, Growth mechanism, "Spheroids", Statistical analysis

Acknowledgements: The research was supported by the PERM SCIENTIFIC AND EDUCATIONAL CENTER "RATIONAL SUBSOIL USE", 2023.

For citation: Petukhov I. V, Medvedeva N. A. Topography and microrelief electroless Ni-P coatings at different loading densities. *Condensed Matter and Interphases*. 2025;27(1): 115–127. http://doi.org/10.17308/kcmf.2025.27/12489

Для цитирования: Петухов И. В., Медведева Н. А. Влияние плотности загрузки на топографию и микрорельеф Ni-P покрытий. *Конденсированные среды и межфазные границы*. 2025;27(1): 115–127. http://doi.org/10.17308/kcmf.2025.27/12489

✉ Igor V. Petukhov, e-mail: petukhov-309@yandex.ru

1. Introduction

Chemically electroless Ni-P coatings have a variety of applications in mechanical engineering, power engineering, and electronics [1] due to the ability to deposit hard, corrosion-resistant, heat-resistant coatings on products of complex configuration and also on dielectrics [2–6].

Currently, optical fiber (OF) is used not only for transmitting information, but also for the production of sensors of various physical quantities (temperature, stress, pressure, etc.) in the oil, gas, and nuclear energy industries [7–10]. Operating conditions of sensors may include temperatures up to 600 °C and aggressive environments. Usually, the OF is produced with a polymer protective and strengthening coating, which protects it from external mechanical influences and moisture [11–12]. Such optical fiber can operate at temperatures up to 200 °C [13]. In order to increase the operating temperature, metallized OF are used, in which a protective and strengthening coating of copper or aluminum is applied directly in the drawing column from molten metal. The operating temperature of such fibers in air is 350–400 °C. However, the copper coating does not sufficiently protect the optical fiber at high temperatures [14]. Nickel-coated optical fiber has higher corrosion resistance [15].

A layer of Ni-P coating can be applied over the metallized copper layer to increase corrosion resistance and heat resistance [16–17]. Such coatings were used in the manufacture of pressure sensors [18]. The coating can be two-layer, a thin layer of Ni-P coating and a thicker layer of electrodeposited nickel [19].

The roughness of the coatings [19–21], determined by the deposition conditions and the composition of the solution, is of great importance. In addition, the lower the roughness of the coatings, the less probable the formation of cavities due to stresses arising from temperature differences [20].

Thus, the application of nickel coatings to metallized optical fiber can be carried out in two ways: electrochemical or electroless nickel plating. In the first case, continuous pulling of the fiber through the nickel plating bath will be required; in the second case, due to the peculiarities of the process, the coating can be applied to a spool of optical fiber. The influence of a number of parameters on the microrelief and growth processes of Ni-P coatings was previously studied [22–25]. In electroless deposition, one of the significant factors is the loading density (the ratio of the area of the surface to be coated to the volume of the solution). In this study, the influence of loading density on the roughness and microrelief of Ni-P coatings was investigated using polished steel samples as the model objects.

2. Experimental

The coatings were deposited on polished samples of 20X13 steel and optical fiber with a quartz core diameter of 125 μm and a copper layer thickness of 18 μm. A copper layer was deposited on the optical fiber from the melt directly in the fiber drawing column.

Mechanical polishing of steel was carried out using a STRUERS LaboPol-2 polishing machine. The coatings copy the microrelief of the substrate, therefore, to eliminate the influence of the microrelief of the substrate on the microrelief of the deposited coatings, careful polishing of the substrate was performed.

Initially, polishing was carried out on Sic-Paper grinding wheels of class 220÷1000, which corresponds to a grain size of 50÷10 μm. Next, DiaPro diamond suspensions with particle sizes from 9 to 1 μm (Struers) were used. For the deposition of coatings, only steel samples with R_a (roughness) not exceeding 4 nm were selected.

Coatings were deposited on 20X13 steel samples for the investigation of the topography and microstructure of Ni-P alloys. The size of the samples was determined by the loading density, which varied from 0.5 to 3.0 dm^2/l.

Before deposition, the samples were degreased with alcohol, washed with distilled water and pickled in HCl (1:1) for 30–60 s. Deposition was carried out at 358 K under thermostatted conditions from a solution of the following composition, (M): $NiCl_2$ – 0.12; NaH_2PO_2 – 0.114; CH_3COONa – 0.12. The temperature was maintained with an accuracy of ±1°, the pH of the solution was 4.5. The reagents for the preparation of solutions were of chemically pure and analytical reagent grade (NaH_2PO_2) and were recrystallized twice. The required pH value was set by adding HCl (extra pure grade).

The thickness of Ni-P coatings on optical fiber was 3.5–4.0 μm. The plasticity of the optical fiber decreased with a higher coating thickness.

The coating thickness was determined gravimetrically, taking the coating density for Ni-P deposits to be 8.0 g/cm^3 [1].

The growth of the coatings and their phosphorus content were studied using a Hitachi S3400N scanning electron microscope and New View-7300 non-contact profilometer (Zygo). The following parameters were analyzed: *PV* – the maximum difference in height between the highest and lowest points of the profile surface; R_A - roughness, *rms* – standard deviation from the central line, R_z – the average absolute value of the five highest peaks and the five deepest depressions. The phosphorus content in the coatings was determined using energy dispersive analysis.

In addition, the average radii ($\bar{r}$), heights of "spheroids" ($\bar{h}$) and the average ratio of these values $\left(\overline{\frac{r}{h}}\right)$ were determined directly from the obtained microprofiles. The analysis of the obtained results was carried out using the MS Excel package. The confidence probability was adopted equal 0.95 for calculations of confidence intervals.

3. Results and discussion

Electroless Ni-P coatings on the surface of the optical fiber must be uniform (Fig. 1a), with a smoothed microstructure and low roughness, which in turn is determined by the deposition conditions, the composition of the elecrtoless nickel plating solution and the loading density. The microrelief of the coatings is determined by the presence of "spheroids" on the surface (Fig. 1b). These are formations elongated in the plane of the substrate with a fairly high ratio of the radius to the height of the "spheroid" [22–23].

The usually used loading density for deposition of coatings does not exceed 2.0 dm^2/l [1]. The study considers the influence of this technological parameter on the growth processes of Ni-P coatings.

The deposition rate had a steady tendency to decrease with an increased loading density (Table 1), which was described earlier [1].

The deposition rate decreased almost twofold with an increase in loading density from 0.5 to 3.0 dm^2/l (Table 1). Starting from a loading density of 1.0 dm^2/l the decrease in deposition rate with increasing loading density occurred almost linearly. An increase in the loading density caused a rapid decrease in the pH of the electroless nickel plating solution (Table 1), a decrease in the concentration of nickel ions and the reducing agent, thus the deposition almost stopped after some time. This was evidenced by a comparison of the dependences of the coating thickness obtained with deposition times of 40 and 60 min (Fig. 2). At a loading density of 3.0 dm^2/l the thickness of the coatings were almost identical.

The substrate had a significant influence on the topography of the growing coatings, since

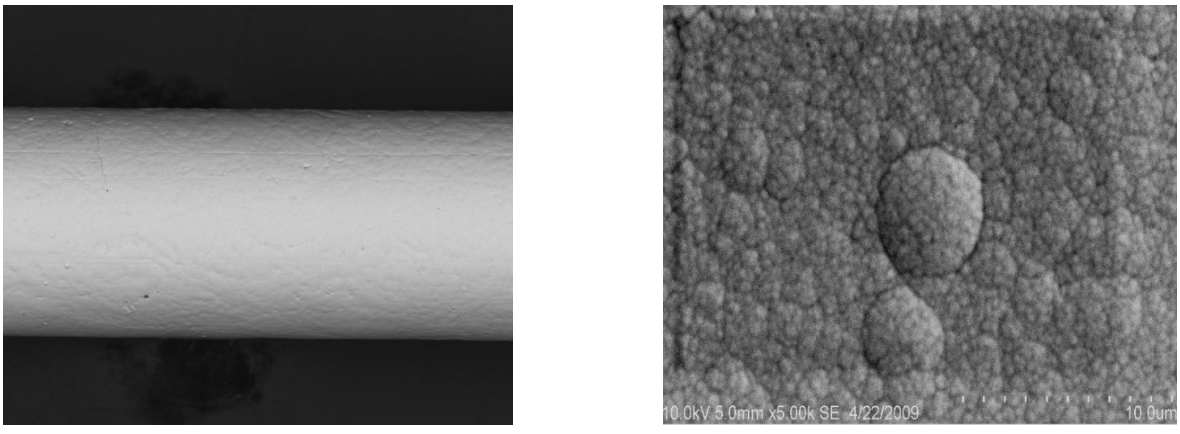

a b

Fig. 1. (a) Micrograph (250x magnification) of Ni-P coating on the surface of copper protective layer on the optical fiber, and (b) "spheroidal" structure of coating (5000× magnification)

Table 1. Coating deposition rate, phosphorus content and change in pH value of electroless nickel plating solution (ΔpH) after deposition at different loading densities

Loading, dm^2/l	Deposition rate, μm/h	Phosphorus content, wt. %	ΔpH
0.5	13.6±1.2	8.1±0.4	0.24±0.06
1.0	13.1±0.5	8.7±0.2	0.39±0.04
1.5	11.9±0.6	9.4±0.2	0.48±0.05
2.0	9.9±0.5	9.8±0.3	0.72±0.07
3.0	7.5±0.5	10.7±0.4	0.85±0.04

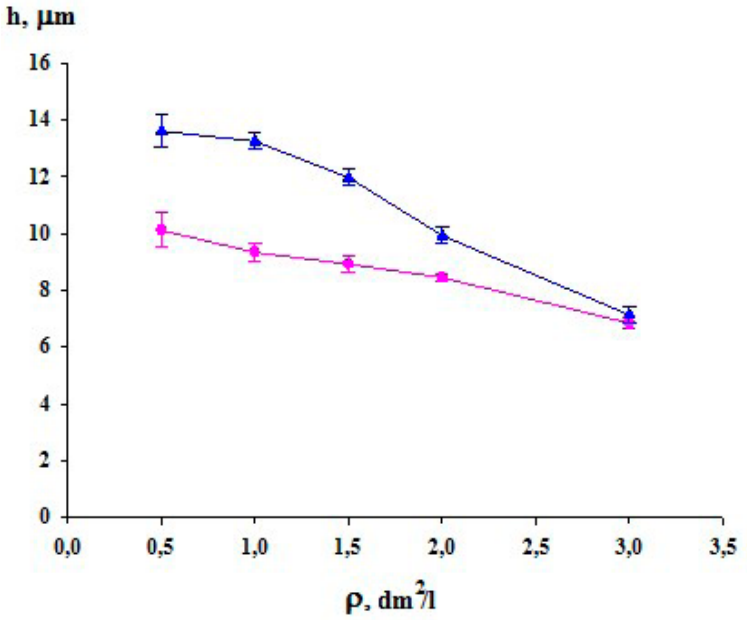

Fig. 2. Dependence of the coating thickness on the loading. Deposition time, minutes: 40 (●), 60 (▲)

Ni-P coatings accurately copied all the details of the substrate surface relief. The decrease in the deposition time will result in a reduction in the coating thickness, which may cause the substrate microrelief to affect the coating's surface topography. Taking this into account, the deposition duration in further studies was 60 min. Deposition at minimum loading density (0.5 dm^2/l) led to the formation of a typical surface relief of Ni-P coatings (Fig. 3). The surface of the coating contained numerous "spheroids", most of which overlapped into agglomerates of various shapes. At the same time, the surface relief was quite smooth, since the height of most "spheroids" did not exceed 30-40 nm.

Increase in the loading density did not qualitatively change the surface topography of the coatings (Fig. 4). The number of "spheroids" on the surface of the coating increased, they become smaller and formed agglomerates of various shapes. For this reason, the detection of clearly distinguishable spheroids was a difficult task.

Individual pores on the surface were detected on the surface, probably formed as a result of the adsorption of hydrogen bubbles, which prevented the deposition of the coating in this area.

The formation of grooves with a linear shape on the surface can probably be associated with the paths of hydrogen bubble removal from the coating surface. Another reason for their occurrence may be insufficient polishing of the steel substrate.

Increase in loading density up to 2 dm^2/l led to an increase in the radii of the "spheroids", which can be concluded from a comparison of the micrographs (Figs. 4 and 5). At the same time, the height of the "spheroids" became

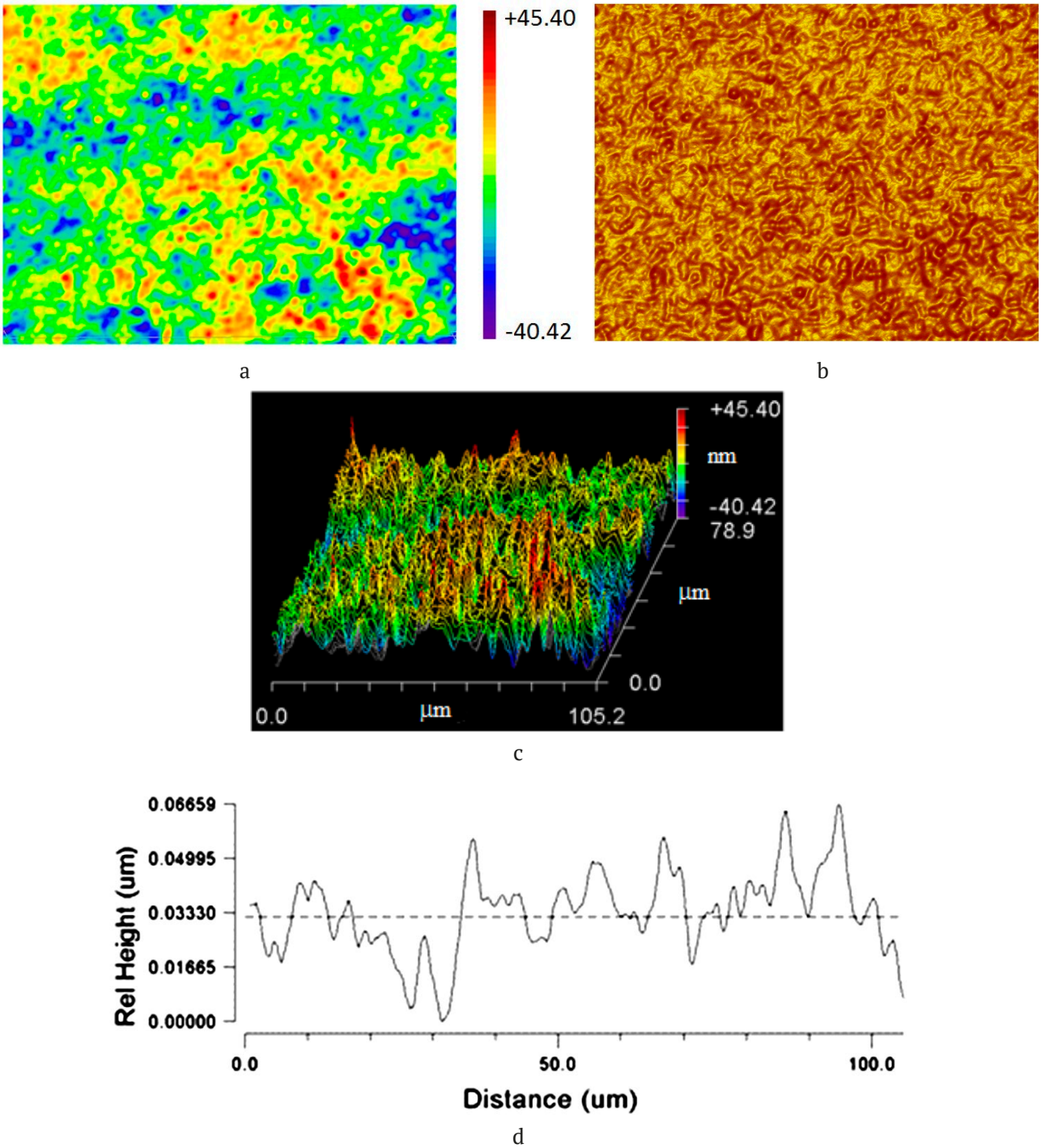

Fig. 3. Topography and microrelief of the coating formed at loading of 0.5 dm^2/l: a – topographical height map; b – map of gradient; c – 3D image of the surface; d – microprofile along the selected direction

smaller. The topography and microrelief of the growing coating did not change fundamentally at the maximum loading density in our series of experiments of 3.0 dm^2/l; in addition to the "spheroids", the same characteristic structural elements – pores and linear grooves.

For a more detailed comparison of roughness, the roughness parameters of the coatings obtained at the studied loading densities were analyzed (Table 2).

The comparison of the microroughness parameters of the coatings indicates that with an

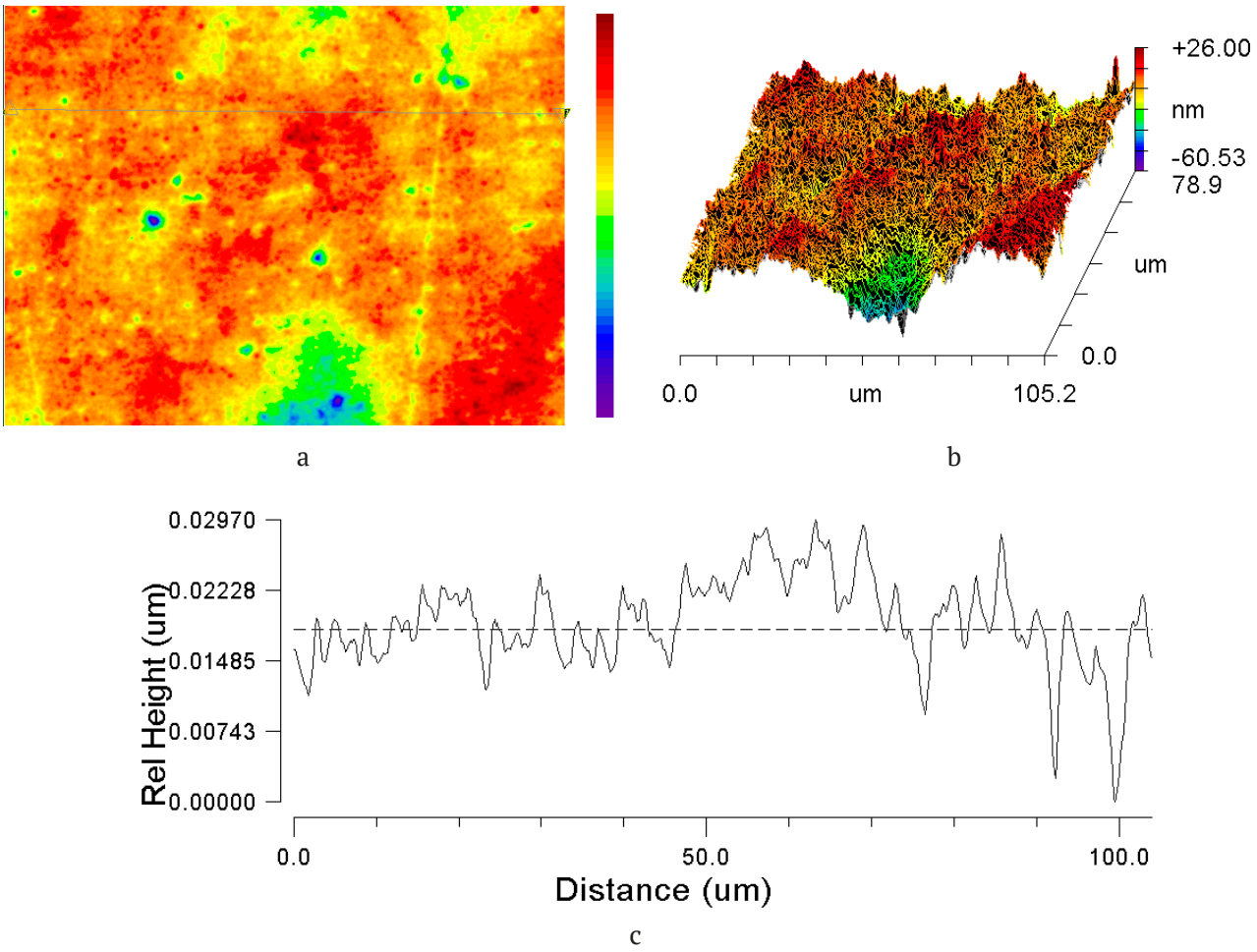

Fig. 4. Topography and microrelief of the coating formed at loading of 1 dm²/l: a – topographical height map; b – 3D image of the surface; c – microprofile along the selected direction

Table 2. Parameters of microroughness of Ni-P coatings, formed at different loadings

Loading, dm²/l	R_a, nm	*rms*, nm	R_z, nm	*PV*, nm
0.5	8.5±2.1	10.8±2.6	54.7±23.9	81.1±17.4
1.0	7.1±1.4	9.3±1.5	62.5±4.9	95.6±12.6
2.0	4.7±1.2	6.2±1.6	26.8±1.3	50.3±7.4
3.0	5.2±1.3	7.4±0.3	51.3±16.6	72.5±25.0

increase in the loading density, the roughness of the coatings did not tend to increase. Moreover, the parameters of microroughness of the coatings obtained at a loading density of 2.0 dm²/l were minimal in the studied series of samples.

At a loading density of 3.0 dm²/l, the microroughness parameters were also comparatively low. Some increase of parameters was possibly due to the fact that at a given loading density, localization of coating growth occurred at the end of deposition. This caused the appearance of irregularly shaped formations on the coating surface with a height of ~100 nm, protruding above the rest of the smoothed surface (Fig. 6). The approximate diameter of such formations was 100–250 μm.

The reason for the occurrence of such formations may be due to the low rate of the deposition process, the surface of the coating does not have time for renewal, and is poisoned by impurity compounds adsorbed from the solution. Only separate areas of the growing surface remain active, which causes localization of the growth of the coating.

Since the process of coating growth occurred through the formation of "spheroids", further treatment of the results consisted of finding the

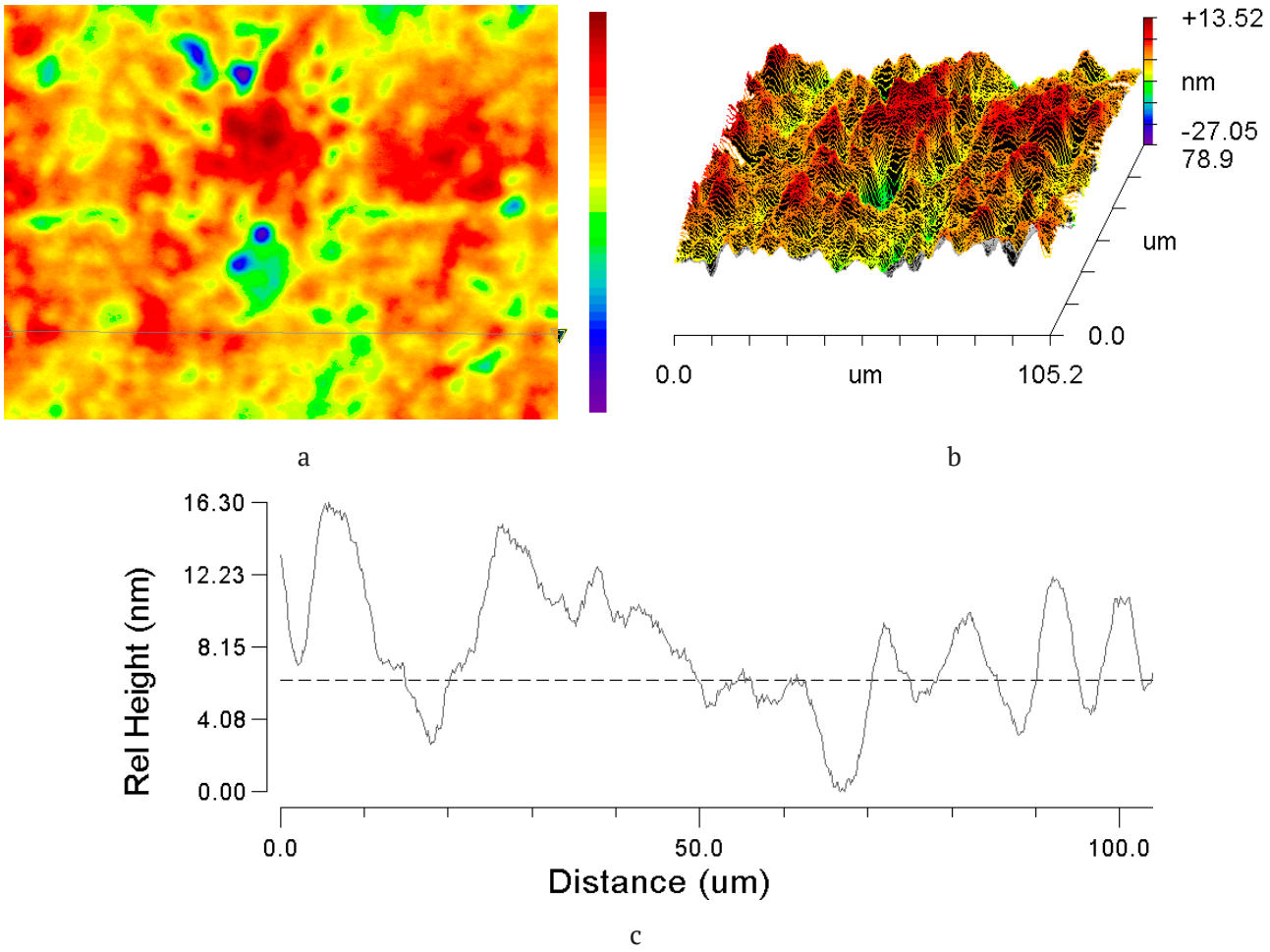

Fig. 5. Topography and microrelief of the coating formed at loading of 2 dm²/l: a – topographical height map; b – 3D image of the surface; c – microprofile along the selected direction

average values of the height ($\bar{h}$), the radius of the "spheroids" ($\bar{r}$) and the relationship of these parameters $\left(\overline{\frac{r}{h}}\right)$ (Fig. 7) based on profilograms. For processing fragments of profilograms where the "spheroids" clearly did not overlap were used.

The average values for each of the loading densities were obtained by averaging several samples, each of which yielded from 70 to 200 experimental values. The results of the treatment are presented in Table 3.

As can be seen from Table 3, changes of the parameters $\bar{h}$, $\bar{r}$, and the $\left(\overline{\frac{r}{h}}\right)$ ratio were non-monotonic. With increasing loading density up to 1 dm²/l the radii and heights of the "spheroids" decreased, while the $\left(\overline{\frac{r}{h}}\right)$ ratio practically did not change. The latter circumstance indicates a similar nature of growth of the coatings. At the same time, the decrease in the average radii and heights of the "spheroids" may be associated with an increase in passivation phenomena during the growth of the coating. A higher loading density caused more intensive acidification of the near-electrode layer of the solution, a decrease in the deposition rate, and increased inhibition of the deposition process by products.

Further increase in loading density up to 2.0 dm²/l led to a noticeable increase in the radii of the "spheroids" with a slight decrease in their heights. These opposite trends in the change of the parameters of the "spheroids" significantly increased the $\left(\overline{\frac{r}{h}}\right)$ ratio.

One of the probable reasons for the increase in the radii of the "spheroids" may be the insufficient

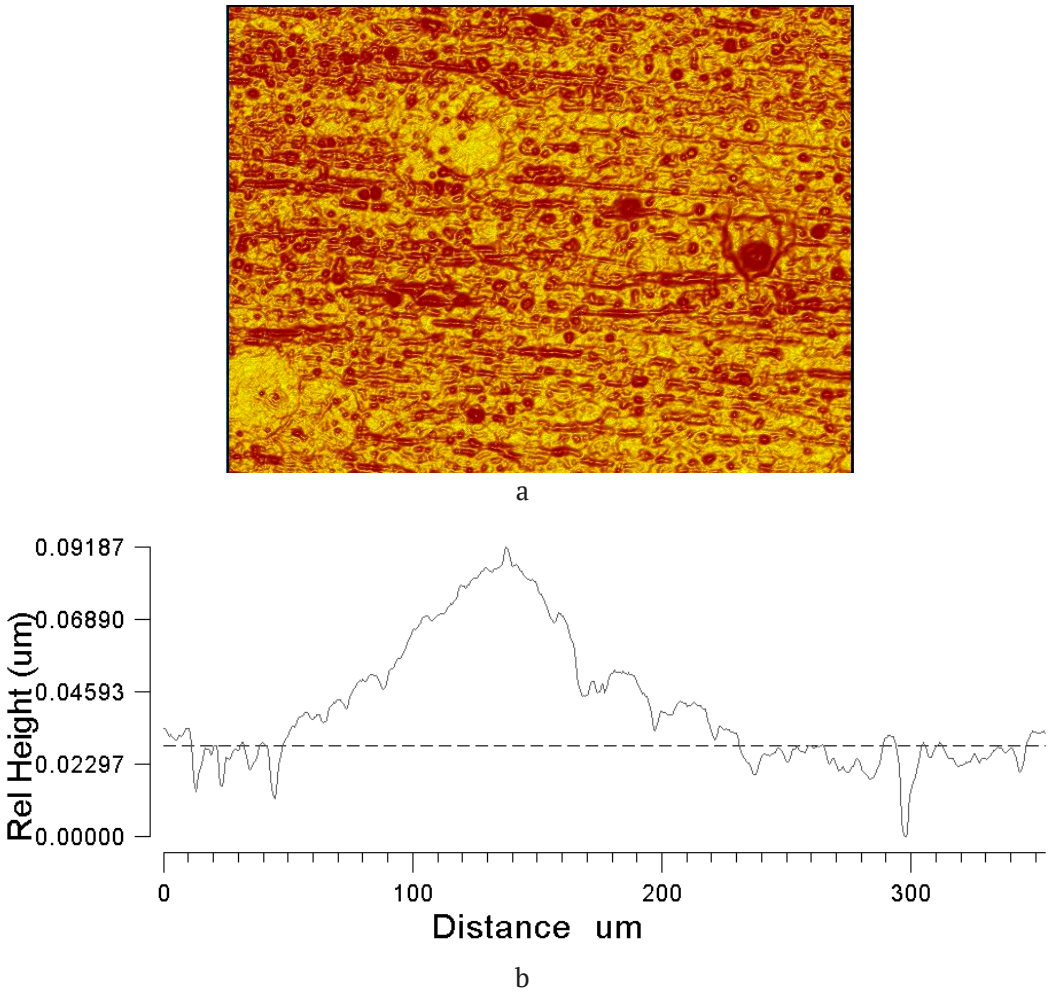

Fig. 6. Topography and microrelief of Ni-P coatings obtained at the loading of 3.0 dm²/l: a – map of gradient; b – microprofile along the selected direction

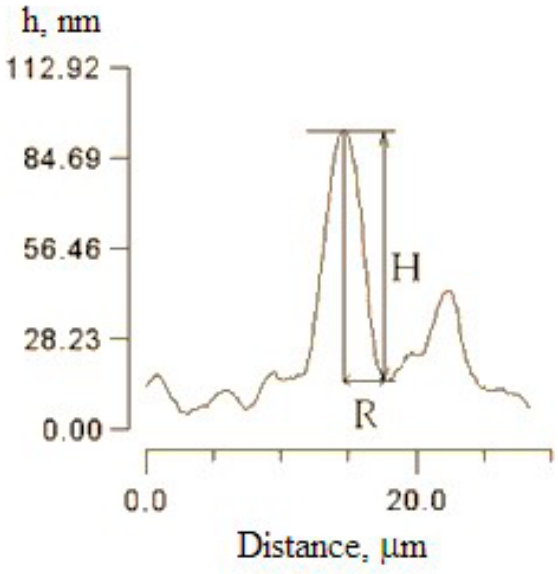

Fig. 7. The scheme of profilogram treatment

resolution of interference microscopy and 3D profilography methods for the study of the fine structure of the resulting "spheroids". It is possible that the "spheroids" observed under these conditions were aggregates of smaller "spheroids". The complex structure of "spheroids" was indicated by the results obtained by the AFM method [25–27]. At the same time, it cannot be ruled out that under conditions of sufficiently low catalytic activity of coating and a low deposition rate, the only possibility for growth was growth in the horizontal direction, which allows the generation of a juvenile coating surface. Similar phenomena were observed during the growth of coatings in the presence of stabilizing additives [23].

A decrease in the radii and the $\overline{\left(\frac{r}{h}\right)}$ ratio with a slight change in the height of the "spheroids"

Table 3. Parameters determined the size of "spheroids" and their growth rates in vertical plane (V_v) and substrate plane (V_s)

Loading, dm²/l	$\bar{r}$, μm	$\bar{h}$, nm	$\overline{\left(\frac{r}{h}\right)}$	$V_г$, nm/s	$V_в$, nm/s
0.5	2.77±0.14	21.22±1.46	143±9	880±46	6.74±0.44
1	1.53±0.08	11.1±0.7	155±9	994±59	6.40±0.01
2	3.63±0.26	8.1±0.7	478±29	2319±139	4.85±0.01
3	2.35±0.18	10.7±1.4	264±26	1073±107	4.05±0.01

was observed at a loading density of 3.0 dm²/l (Table 3).

Despite the complex nature of the change in the parameters of the "spheroids", we attempted to use the layered growth mechanism to describe their growth processes [22-23, 25]. Within the framework of this mechanism, the average growth rates of "spheroids" in the lateral (V_h) and normal directions (V_v) were determined (Table 3).

Analysis of the results shown in Table 3 indicates that increasing the loading density decreased the rate of normal growth. It should be noted that its increase from 0.5 to 1.0 dm²/l had a relatively weak effect on growth rates in both normal and lateral directions.

The main reason for the decrease in normal growth rate was the acidification of the electroless nickel plating solution during the deposition process (Table 1). The acidification of the surface layer of the solution was even more expressed [28]. These changes in the composition of the solution blocked vertical growth.

The decrease in normal growth rate with a decreasing pH of the solution has been described previously [23]. Acidification of the solution with increasing loading density should also lead to a decrease in lateral growth, but the results indicated an increase in the growth rate of the "spheroids" in this direction. This was probably due to the fact that in this case, using profilometric measurements, we recorded the dimensions of not a single "spheroid", but a formation composed by several "spheroids".

Further processing of the obtained results consisted of statistical analysis of samples of radii and heights of "spheroids", *r*/*h* ratio for each of the studied loading densities.

For each loading density, histograms of the spheroid size distribution were obtained (separately, histograms of the distribution by *r* and *h*), and the distribution of the ratio of these values (*r*/*h*). Histograms of the distribution of the values of *r*, *h* and the *r*/*h* ratio for coatings obtained at different loading densities are shown in Figs. 8–9.

In order to assess the compliance of the obtained distributions with the normal law, the values of the coefficients of asymmetry (γ_1^*), excess (γ_2^*) and the values of these coefficients acceptable for the normal distribution were calculated [28]:

$$\left|\gamma_1^*\right| \le \gamma_{1,\text{norm}}^*, \quad (1)$$

$$\left|\gamma_2^*\right| \le \gamma_{2,\text{norm}}^*, \quad (2)$$

Maximum permissible values of asymmetry coefficients $\left(\gamma_{1,\text{norm}}^*\right)$ and excess $\left(\gamma_{2,\text{norm}}^*\right)$ were calculated using the following formulas:

$$\gamma_{1,\text{norm}}^* = 3\sqrt{D\left(\gamma_1^*\right)}, \quad (3)$$

$$\gamma_{2,\text{norm}}^* = 5\sqrt{D\left(\gamma_2^*\right)}, \quad (4)$$

where $D\left(\gamma_1^*\right)$ and $D\left(\gamma_2^*\right)$ – the dispersions of these values determined using the following equations:

$$D\left(\gamma_1^*\right) = \frac{6(n-1)}{(n+1)(n+3)}, \quad (5)$$

Table 4. Statistical parameters of spheroids' radius distribution

Loading, dm²/l	*r*, μm	γ_1^*	γ_2^*	*n*	$\gamma_{1\ \text{normal}}^*$	$\gamma_{2\ \text{normal}}^*$
0.5	2.8±0.1	1.7 6	0.81	142	0.60	1.94
1	1.5±0.1	0.78	1.02	195	0.52	1.68
2	3.6±0.3	-0.11	0.46	82	0.78	2.46
3	2.4±0.2	0.28	0.59	71	0.84	2.62

Table 5. Statistical parameters of spheroids' height distribution

Loading, dm²/l	*h*, nm	γ_1^*	γ_2^*	*n*	$\gamma_{1\ normal}^*$	$\gamma_{2\ normal}^*$
0.5	21.2±1.5	1.10	0.90	142	0.60	1.94
1	11.1±0.7	1.52	1.15	195	0.52	1.68
2	8.1±0.7	1.64	0.95	82	0.78	2.46
3	10.7±1.4	1.25	1.18	71	0.84	2.62

Table 6. Statistical parameters of *r/h* ratio distribution

Loading, dm²/l	*r/h*	γ_1^*	γ_2^*	*n*	$\gamma_{1\ normal}^*$	$\gamma_{2\ normal}^*$
0.5	143±9	1.66	0.81	142	0.60	1.94
1	155±9	22.2	3.69	195	0.52	1.68
2	478±29	8.88	2.57	82	0.78	2.46
3	264±26	0.11	0.51	71	0.84	2.62

$$D\left(\gamma_2^*\right)=\frac{24n(n-2)(n-3)}{(n+1)^2(n+3)(n+5)}. \quad (6)$$

The results of the calculations performed for samples obtained at different loading densities are shown in Tables 4–6.

A comparison of the asymmetry and excess coefficients calculated for a sample of experimental values of the "spheroid" parameters with similar coefficients for a normal distribution allows to conclude that for most loading densities, the distribution of "spheroids" by size does not obey the normal law. Deviations from the normal law are caused by an increase in asymmetry coefficient values. The most heterogeneous is the distribution of the parameter *r/h*. This is obvious even from the appearance of the histograms (Fig. 8c, 9c) without additional statistical processing. The excess coefficient for most cases corresponded to a normal distribution.

The fact that the distribution of "spheroids" by size corresponded to the normal law may indicate that all "spheroids" grow by the same mechanism. The possible simultaneous implementation of normal and layered growth mechanisms was mentioned in [24]. Under the deposition conditions used in the study, no "spheroids" with a low *r/h* ratio were observed, which is typical for the mechanism of normal growth. Therefore, deviations from the normal distribution may be associated with the fact that in a number of cases, instead of individual spheroids, we registered aggregates of these "spheroids". The used method did not provide the required horizontal resolution. In order to obtain the required resolution, atomic

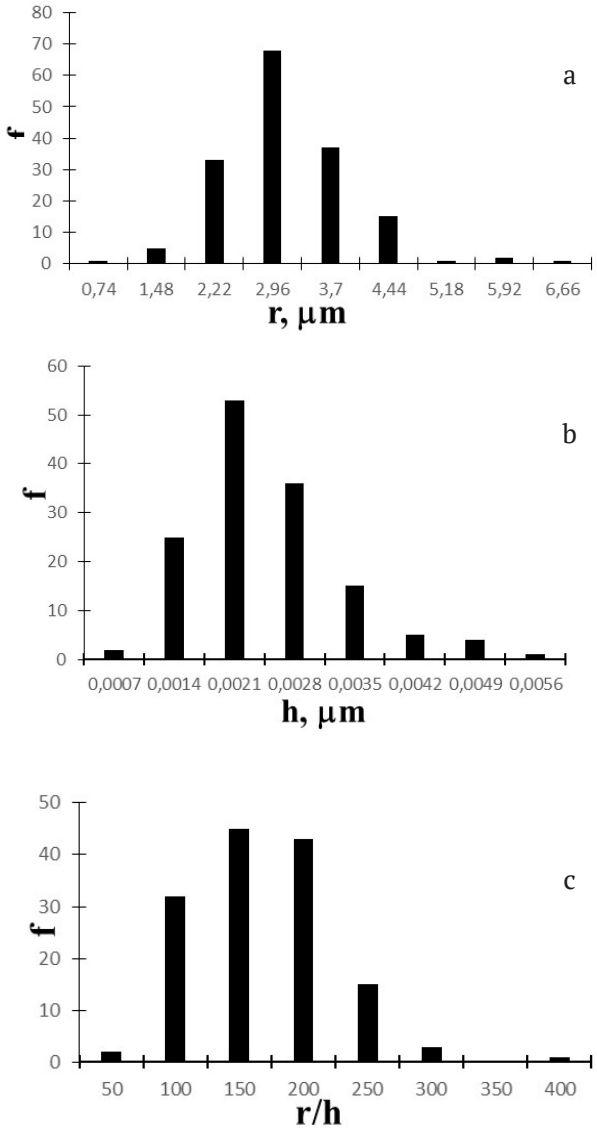

Fig. 8. *r* (a), *h* (b) and *r/h* ratio (c) distributions for spheroids obtained at loading of 0.5 dm²/l

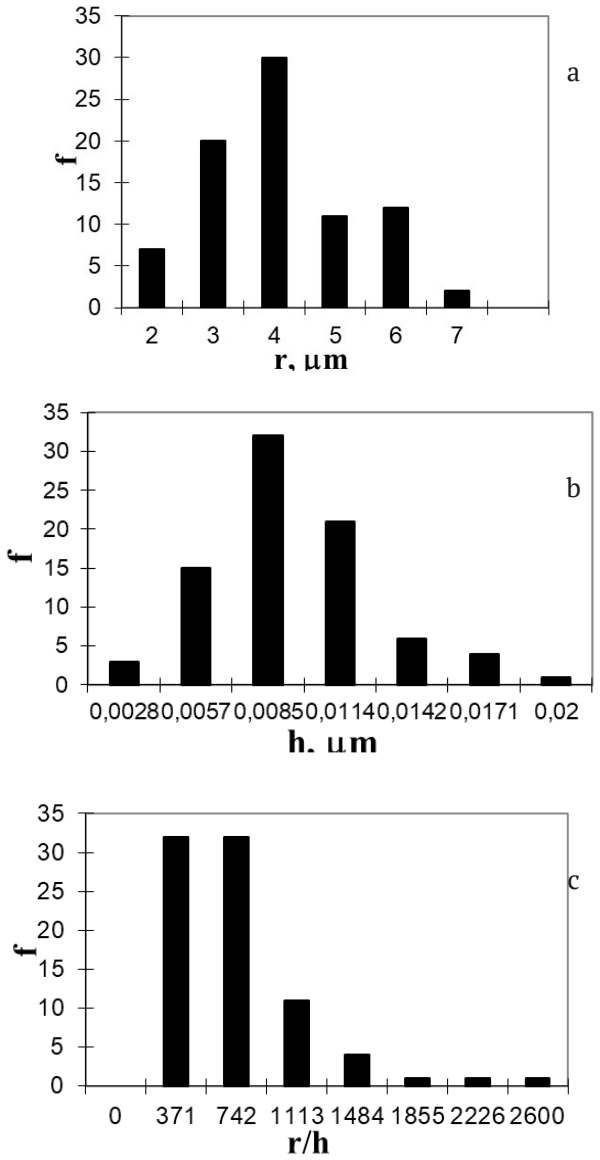

Fig. 9. *r* (a), *h* (b) and *r/h* ratio (c) distributions for "spheroids" obtained at loading of 2.0 dm^2/l

force microscopy should be used, but due to the labor intensity of the method, it will be difficult to obtain a similar sample size. The presence of individual "spheroids" and aggregates of them in one statistical sample may lead to deviations from the normal law.

At the same time, the obtained results do not contradict the layered growth mechanism, since during the coating deposition process, the pH of the electrolyte changes, the deposition rate decreases, which can enhance passivation phenomena on the growing surface. Due to this, the movement of individual atomic layers spreading over the surface can be blocked. For this reason, multiple growth centers (several growth layer packages) arise. These newly formed "spheroids" grow until they overlap with each other (Fig. 1b). In this way the structuring of the growing "spheroid" occurs. The rounded shape of these formations is determined by the fact that at this shape the surface energy is minimal at the spheroid-solution interface, since the amorphous structure of the coatings does not require crystalline faceting. If there is no change in the growth mechanism, it can be assumed that this will not have a significant impact on the calculation results presented in Table 3.

4. Conclusions

Thus, the investigation of growth processes at loading densities from 0.5 to 3.0 dm^2/l allows us to conclude that an increase in the loading density in the studied range of values does not lead to an increase in the roughness of the coatings. Probably, the condition for the transition to the normal growth mechanism and the corresponding increase in the roughness of the coatings is a sufficiently high catalytic activity of the surface accompanied by the discharge of nickel ions in the diffusion or diffusion-kinetic mode, which can occur with an increase in the temperature of the electroless nickel plating solution or with a decrease in the concentration of nickel ions [24].

An increase in the loading density increases the acidification of the electroless nickel plating solution during the deposition process, which contributes to an increase in the phosphorus content in the coatings and, as a consequence, a decrease in their catalytic activity in the oxidation reaction of the reducing agent (sodium hypophosphite), due to which the deposition rate significantly decreases.

Under condition of low deposition rates (low catalytic activity of coatings), conditions for the discharge of nickel ions in diffusion mode and the transition to the normal growth mechanism with the formation of dendritic deposits probably are not created. Therefore, with an increase in loading density, coatings with a smooth surface can be formed.

Some additional increase in roughness occurs only when the deposition rate is reduced to almost zero and the growth process occurs only on individual active areas of the coating surface.

The obtained results should be taken into account when depositing Ni-P coatings on the surface of optical fiber.

Contribution of the authors

The authors contributed equally to this article.

Conflict of interests

The authors declare that they have no known competing financial interests or personal relationships that could have influenced the work reported in this paper.

References

1. *Electroless nickel plating*: fundamentals to applications. Delaunois F., Vitry V., Bonin L. (eds.). *CRC Press*. 2019: 446. https://doi.org/10.1201/9780429466274

2. Sudagar J., Lian J., Sha W. Electroless nickel, alloy, composite and nano coatings – a critical review. *Journal of Alloys and Compounds*. 2013;571(15): 183–204. https://doi.org/10.1016/j.jallcom.2013.03.107

3. Chintada V. B., Koona R., Raju Bahubalendruni M. V. A. State of art review on nickel-based electroless coatings and materials. *Journal of Bio- and Tribo-Corrosion*. 2021;7(4): 1–14. https://doi.org/10.1007/s40735-021-00568-7

4. Muraliraja R., Selvan R. A. S., … Sudagar J. A review of electroless coatings on non-metals: Bath conditions, properties and applications. *Journal of Alloys and Compounds*. 2023;960: 170723. https://doi.org/10.1016/j.jallcom.2023.170723

5. Biswas P., Das S. K., Sahoo P. Investigation of tribological and corrosion performance of duplex electroless Ni-P/Ni-Cu-P coatings. *Materials Today: Preceedings*. 2023;80(2): 1122–1129. https://doi.org/10.1016/j.matpr.2022.12.119

6. Oh S., Kim D., Kim K. Ch., Kim D.-I., Chung W., Shin B.-H. Electrochemical properties of electroless Ni plated super duplex stainless in 3.5% NaCl solution. *International Journal of Electrochemical Science*. 2023;18(10): 100287. https://doi.org/10.1016/j.ijoes.2023.100287

7. Lee B. Review of the present status of optical fiber sensors. *Optical Fiber Technology*. 2023;9: 57–79. https://doi.org/10.1016/S1068-5200(02)00527-8

8. Engelbrecht R. Fiber Optic strain and temperature sensing: overview of principles. *Proceedings Sensor*. 2017: 255–260. https://doi.org/10.5162/sensor2017/B6.1

9. Li J., Sun X., Huang L., Stolov A. Optical fiber for distributed sensing in harsh environments. *Fiber Optic Sensors and Applications XV, 13*. 2017; 106540E. https://doi.org/10.1117/12.2305433

10. Liu H. H., Hu D. J. J., Sun Q., … Shum P. P. Specialty optical fibers for advanced sensing applications. *Opto-Electronic Science*. 2023;2(2): 220025. https://doi.org/10.29026/oes.2023.220025

11. Salunkhe T. T., Kim I. T. Sequential dual coating with thermosensitive polymers for advanced fiber optic temperature sensors. *Sensors*. 2023;23(6): 2898. https://doi.org/10.3390/s23062898

12. Janani R., Majumder D., Scrimshire A., … Bingham P. A. From acrylates to silicones: a review of common optical fibre coatings used for normal to harsh environments. *Progress in Organic Coatings*. 2023;180: 107557. https://doi.org/10.1016/j.porgcoat.2023.107557

13. Popelka M., Stolov A. A., Hokansson A. S., Li J., Hines M. J. A new polyimide coating for optical fibers: demonstration of advantageous characteristics in harsh environments. *Optical Components and Materials XIX*. 2022;11997: 119970J. https://doi.org/10.1117/12.2608322

14. Popov S. M., Voloshin V. V., Vorobyov I. L., … Chamorovski Y. K. Optical loss of metal coated optical fibers at temperatures up to 800 °C. *Optical Memory and Neural Networks (Information Optics)*. 2012;21(1): 45–51. https://doi.org/10.3103/S1060992X12010080

15. Lupi C., Vendittozzi C., Ciro E., Felli F., Pilone D. Metallurgical aspects of Ni-coating and high temperature treatments for FBG spectrum regeneration. *Materials*. 2023;*16*(8): 2943. https://doi.org/10.3390/ma16082943

16. Filas R. W. Metallization of silica optical fiber. *MRS Proceedings*. 1998;531: 263–268. https://doi.org/10.1557/PROC-531-263

17. Wysokiński K, Stańczyk T., Gibała K., … Nasiłowski T. New methods of enhancing the thermal durability of silica optical fibers. *Materials*. 2014;7: 6947–6964. https://doi.org/10.3390/ma7106947

18. Rosolem J. B., Penze R. S., Bassan. F. R., … Junior M. A. R. Electroless nickel-plating sealing in FBG pressure sensor for thermoelectric power plant engines applications. *Journal of Lightwave Technology*. 2019;37(18): 4791–4798. https://doi.org/10.1109/JLT.2019.2920120

19. Mei X., Jiang B. Thick nickel coating on surface of quartz optical fiber by electrochemical deposition method. *Applied Mechanics and Materials*. 2015;727-728: 51–55. https://doi.org/10.4028/www.scientific.net/AMM.727-728.51

20. Shiuea Sh.-Ts., Yang C.-H., Chub R.-Sh., Yang Ts.-J. Effect of the coating thickness and roughness on the mechanical strength and thermally induced stress voids in nickel-coated optical fibers prepared by electroless plating method. *Thin Solid Films*. 2005;485: 169–175. https://doi.org/10.1016/j.tsf.2005.04.024

21. Huang L., Wang Zh., Li Zh., Deng W.. Electroless nickel plating on optical fiber probe. *Chinese Optics Letters*. 2009;6: 472–474. https://doi.org/10.3788/COL20090706.0472

22. Petukhov I. V. Of the mechanism governing the growth of electrolessly deposits nickel-fhosphorus coatings. *Russian Journal of Electrochemistry*. 2007;43(1): 34–41. https://doi.org/10.1134/S1023193507010053

23. Petukhov I. V. The effect of component concentration in electroless nickel plating soluton on topography and microeliefof Ni-P coatings. *Russian Journal of Electrochemistry*. 2008;44(2): 147–157. https://doi.org/10.1007/s11175-008-2002-9

24. Petukhov I. V., Medvedeva N. A., Mushinskii S. S., Nabiullina M. R. Possible reasons for the appearance of metallic phase in electroless nickel plating solutions. *Russian Journal of Applied Chemistry*. 2012;85(1): 29–34. https://doi.org/ 10.1134/S1070427212010065

25. Petukhov I. V., Semenova V. V., Medvedeva N. A., Oborin V. A. Effect of deposition time on the formation of

Ni-P coating. *Bulletin of Perm University. CHEMYSTRY*. 2011;3(3): 47–56. Available at: https://www.elibrary.ru/item.asp?id=17563299

26. Wang J-Y., Peng B., Xie H-N., Cai W.-B. In situ ATR–FTIR spectroscopy on Ni–P alloy electrodes. *Electrochimica Acta*. 2009;54(6): 1834–184. https://doi.org/10.1016/j.electacta.2008.10.015

27. Elansezhian R., Ramamoorthy B., Kesavan N. The influence of SDS and GTAB surfactants on the surface morphology and surface topography of electroless Ni-P deposits. *Journal of Materials Processing Technology*. 2009;209: 233-240. https://doi.org/10.1016/j.jmatprotec.2008.01.057

28. Vashkyalis P.-A. Yu. *Regularities and mechanism of autocatalytic reduction of metals in aqueous solutions**. Dr. chem. sci. diss. Vilnius: 1982. 405 p. (In Russ.)

29. Akhnazarova S. L., Kafarov V. V. *Optimization of experiments in chemistry and chemical technology**. Moscow: Vysshaya Shkola Publ.; 1978. 319 p. (In Russ.)

** Translated by author of the article*

Information about the authors

Igor V. Petukhov, Cand. Sci. (Chem.), Associate Professor at the Department of Physical Chemistry, Perm State University (Perm, Russian Federation).

https://orcid.org/0000-0002-3110-668x

petukhov-309@yandex.ru

Natalia A. Medvedeva, Cand. Sci. (Chem.), Associate Professor, Head of the Department of Physical Chemistry, Perm State National Research University (Perm, Russian Federation).

https://orcid.org/0000-0002-0042-5418

nata-kladova@yandex.ru

Received 19.10.2023; approved after reviewing 18.04.2024; accepted for publication 15.05.2024; published online 25.03.2025.

Translated by Valentina Mittova